Photochemical & Photobiological Sciences

Accepted Manuscript

This article can be cited before page numbers have been issued, to do this please use: B. Finkler, I. Riemann, M. Vester, A. Grüter, F. Stracke and G. Jung, *Photochem. Photobiol. Sci.*, 2016, DOI: 10.1039/C6PP00290K.

ROYAL SOCIETY OF CHEMISTRY

rsc.li/pps

View Article Online
DOI: 10.1039/C6PP00290K

Monomolecular Pyrenol-Derivatives as Multi-Emissive Probes for Orthogonal Reactivities

Björn Finkler[a], Iris Riemann[b], Michael Vester[a], Andreas Grüter[a], Frank Stracke[b], Gregor Jung[a]*

[a] Biophysical Chemistry, Saarland University, Campus B2 2, 66123 Saarbrücken, Germany.

[b] Fraunhofer-IBMT, Ensheimer Straße 48, 66386 St. Ingbert, Germany.

*E-mail: g.jung@mx.uni-saarland.de. Fax: +49 (0)681 302 64846. Phone: +49 (0)681 302 64848.

Abstract: Photoacids on basis of pyrenol have been extensively studied in the past 60 years. As their photophysical properties strongly depend on the substituents at the aromatic scaffold, we introduced two reactive moieties with different electronic coefficients thus creating multi-wavelength fluorescent probes. One probe is capable of monitoring two orthogonal transformations by four fluorescence colors, distinguishable even by the naked human eye. Another derivative can act as three-color sensor for a wide range of different pH values. Both presented compounds allow for mimicking fundamental and advanced two-input logic operations due to the multi-wavelength emission. Furthermore, these compounds can process information in a logically reversible way (Feynman gate).

Introduction

Information processing with optical probes enables rapid and sensitive detection of different analytes in biochemical and supramolecular systems.[1–3] Fluorogenic substrates, *i.e.* a logic YES-gate, are widely used for the detection and activity determination of enzymes due to the high sensitivity of fluorescence based methods.[1,4–9] Yet, measurements with *on-off* probes impose complications in quantification[10,11], which are largely overcome by use of dual-emissive probes, *i.e.* a YES and a NOT gate in a single molecule.[2,3,11–16] Enzymes with their fundamental importance for the function of biological systems are one of the key objectives of these probes. Since multianalyte systems are promising tools for "smart" medical diagnostics[17–20], probes for multiple enzymes are of particular interest. So far, only few single probes for two enzymes were reported.[17,21–23] Most of these examples are fluorogenic since they emit only fluorescence if both enzymes are present and can monitor only a combined activity of both enzymes. When only one or the other enzyme is present, these systems provide no information. A separate single enzyme probe would be necessary to address this

View Article Online
DOI: 10.1039/C6PP00290K

scenario. One notable exception that enables resolution of individual enzyme activity with a cleavable FRET-pair is presented by Li *et al.*.[21] While the fluorogenic probes can be seen as AND gates, this latter example "has to be regarded as an OR logic gate"[22], since a clear assignment of the corresponding metabolization states to the emission spectra is demanding for this probe. Here we present the ratiometric, monomolecular dual enzyme probe **1**. The probe utilizes the spectral differences of photoacid and corresponding base as well as the sensitivity of the pyrene based photoacids to modifications which alter the electron-withdrawing strength of the aromatic substituents. Our system exhibits four distinct metabolization states denoted by four easily distinguishable fluorescence colors. Since phosphatase activity is an important marker for several human diseases[13,24,25] and carboxyl esterase plays a key role in detoxification processes and drug targeting[12,16,26], these enzymes were chosen as target. Furthermore, a multi-wavelength sensor for a wide range of different pH values is introduced which is also based on the same system as probe **1**. On top, both derivatives can mimic Boolean operations like AND or INHIB[27–29] and even more advanced logic operations.

Results and Discussion

Synthesis

Scheme1

Scheme 1 illustrates the synthetic pathway yielding compounds **1**-**4**. In the first step 1-pyrenol was selectively mono-brominated at the distal ring. The mixture of both regioisomers **5** was subsequently transformed into the corresponding disulfonamides **6**. After reaction with benzyl bromide, the two isomers could be separated by preparative column chromatography. For further synthesis, solely derivative **7** was used, of which the substitution pattern was confirmed by X-ray crystallographic analysis (see ESI S17-S20). Subsequently, the bromine atom was transformed in a palladium-catalyzed carbonylation to the carboxylic ethyl ester **8**. The hydroxyl group was then deprotected via palladium-catalyzed transfer hydrogenation yielding **2**. The dual enzyme sensor **1** was synthesized by reaction of **2** with phosphoroxy chloride and subsequent hydrolysis of the resulting dichloride in a water/acetone mixture in an overall yield of 10% over six steps. Additionally, the expected products of an enzymatic hydrolysis (**3** and **4**) were synthesized for comparison. The multi-wavelength pH-sensor compound **4** was obtained upon alkaline hydrolysis of **2** with potassium *tert*-butoxide in

View Article Online
DOI: 10.1039/C6PP00290K

presence of water according to the procedure of Gassman *et al.*[30], and compound **1** was hydrolyzed in a weakly alkaline aqueous solution to yield **3**.

Since the hydroxyl group and the opposite position of the aromatic system are the substitution sites inducing spectral changes to distinctly different extents, derivatives for other analytes can be created by variation of two of the six reaction steps (Scheme 1). Furthermore, compounds **1**-**4** exhibit high photostability (see ESI S38), long fluorescence lifetimes and quantum yields of at least 85% (Table 1 and 3) which qualifies them as powerful tools for ultrasensitive fluorescence spectroscopy.

Dual enzyme substrate

Pyrenol and especially its sulfonated derivatives are classified as photoacids.[31–33] If these molecules are electronically excited, the observed fluorescence mainly results from the conjugated base formed by excited-state proton transfer (ESPT) and is bathochromically shifted compared to the conjugated acid for electronic reasons. The corresponding base can also be excited directly at pH values above the ground state pK_a. Introduction of electron-withdrawing groups into the aromatic system is a common way to tune the photophysical properties of photoacids.[34–43] Hence, we introduced a cleavable carboxylic ester into the pyrene scaffold (**1** and **2**). The carboxylic ethyl ester (R-CO_2Et) exhibits a Hammett σ_p-value, a convenient measure of electron-withdrawing property, of 0.45[44] whereas carboxylate (R-CO_2^-) at a physiological pH is less electron-withdrawing (σ_p = 0.00).[44] Thus, fluorescence emission of the hydrolysis products (**3** and **4**) is blue shifted compared to **1** and **2**, respectively (Figure 1). A substrate for phosphatases is obtained by conversion of the hydroxyl-group to a phosphate monoester (**1** and **3**). At physiological pH, hydrolysis of this group results in a strongly red shifted emission since the emission arises from the corresponding base of compound **2** or **4**, respectively (Figure 1, Table 1). Remarkably, the effects of phosphorylation and esterification are roughly additive on the wavelength scale.

Figure1

Table 1

Enzymatic hydrolysis of **1** by porcine liver esterase (PLE) shifts the emission from λ_{em} = 472 nm to λ_{em} = 448 nm. Upon dephosphorylation by alkaline phosphatase (AlP), fluorescence is shifted from λ_{em} = 472 to λ_{em} = 558 nm. When both enzymes are present, their combination

View Article Online
DOI: 10.1039/C6PP00290K

induces an emission maximum at λ_{em} = 536 nm. Precise comparison of the spectroscopic data with the reference compounds **2-4** confirms that indeed these products are formed by the intended enzymatic reactions. Kinetic parameters of the enzyme reactions were determined via fluorescence spectroscopy using a Lineweaver-Burk plot (see ESI S39-S44). As reference substrates, commercial available 4-methylumbelliferyl phosphate (4-MUP)[45] *resp.* butyrate (4-MUBu)[46] were used. The determined K_m values for the enzymatic hydrolysis of 4-MUP by AlP (Table 2) under the used assay conditions are in a similar range as those determined by Fernley *et al.*.[45]

Table 2

The determined K_m values (Table 2) characterize **1** (K_m = 3.0 x 10^{-6} M) and **3** (K_m = 2.9 x 10^{-6} M) as good substrates for alkaline phosphatase comparable to the fluorogenic reference compound 4-MUP under the same assay conditions (K_m = 2.2 x 10^{-6} M). The enzymatic efficiency of these probes, *i.e.* k_{cat}/K_m are also in a similar range as that found for 4-MUP (Table 2). Furthermore, the phosphate hydrolysis of **1** and **3** can also be achieved by acid phosphatase (AP). K_m generally about ten times higher compared to enzymatic hydrolysis with alkaline phosphatase, but k_{cat}/K_m is reduced by several orders of magnitude (Table 2).
K_m values for the ester hydrolysis of **2** by porcine liver esterase are lower by the factor 5 whereas k_{cat}/K_m is roughly 1.3 times higher compared to the 4-methylumbelliferyl substrate 4-MUBu (Table 2), which suggests that **2** is a somewhat better substrate than the commercial fluorogenic probe. While the hydrolysis of **2** to **4** by PLE is rather fast, hydrolysis of **1** to **3** by PLE is decelerated, thus disabling determination of K_m. Hydrolysis rates were similarly slow with carboxylic acid esterase from *Paenibacillus barcinonensis*, which suggests that **1** is not an ideal substrate for carboxylesterases. According to the widely used empirical model proposed by Jones *et al.*[47,48], only the large hydrophobic pocket provides enough space for binding the aromatic core of **1** and **2**. Compared to **2**, **1** is not only sterically more bulky, but also twice negatively charged, which likely causes repulsion from the hydrophobic pocket. As a result, substrate **1** might not be optimally coordinated at the active site and hence, the enzymatic hydrolysis may not be very effective. However, k_{cat}/K_m of AlP and PLE are ordered in such a way that the conversion of **1→2→4** can be easily tracked by fluorescence spectroscopy.

View Article Online
DOI: 10.1039/C6PP00290K

Live-cell application

The dual enzyme sensor **1** was applied to L929 cells (Figure 2; for T 84 cells, see ESI S45). Excitation of **1** and the corresponding metabolites was performed, as previously, with two-photon excitation (λ_{ex} = 800 nm).[43]

Figure 2

As control, cells were incubated with the different possible products of the enzymatic transformation (see ESI S46, S47). Even 24 hours after incubation, no permeation in cells was found for compounds with the free carboxylate group (**3** and **4**), presumably due to the negative charge at this substituent. Besides the absence of membrane penetration of **4**, the corresponding image further shows that no significant autofluorescence was detectable under the used setup conditions. Interestingly, uptake of the negatively charged phosphoric acid monoester **1** into the cell plasma was detectable in each measurement. The transport inside might be facilitated by transporter proteins which are naturally specialized in the exchange of nucleosides[49,50] through the cell membranes.

Fluorescence filters in Figure 2(a, b) and (c, d) were selected to exclusively monitor the phosphatase activity. In the extracellular medium only emission of **1** is detected. After three hours, fluorescence emission of **1** is still detectable in the medium outside the cell, indicating an incomplete uptake and, moreover, the absence of segregated phosphatase. Detection of **1** within the cells suggests that metabolization only occurs after internalization. Emission of the dephosphorylated product **2** measured in the cytosol rises over time and reflects the intracellular phosphatase activity.

After conversion of **1** to **2**, esterase activity was monitored by observation of the hydrolysis of **2** (λ_{det} = 565-615 nm) to **4** (λ_{det} = 500-530 nm). One hour after incubation, fluorescence from **2** is clearly discernible and emission of the hydrolyzed product **4** is only weakly detectable. While emission intensity of **2** was about the same after 3 hours (Figure 2(g, h)), the fluorescence emission of **4** is much more pronounced (Figure 2(e, f)). Similar behavior was previously observed in HeLa cells by use of a carboxyl BODIPY derivative.[16] Beneficially, k_{cat}/K_m of AlP and PLE (Table 2, Figure 1(b)) are ordered in such a way that the uptake and the subsequent conversion of **1→2→4** can be easily monitored by microscopy. It should be

View Article Online
DOI: 10.1039/C6PP00290K

mentioned that **3** can only be detected when phosphatase activity is completely lacking. This is observed in selected areas of T84 cells (ESI Figure S74).

The possible monitoring of the four distinct fluorescent products in the cell clusters enables the application of the above described concepts of molecular logic. For example, after incubation with **1**, the output of the green channel (λ_{det} = 500-530 nm, Figure 2(e, f)) in combination with a suitable threshold value and esterase/phosphatase activity as inputs represents an AND gate within the cell cluster similarly as previously shown.[22] In contrast to fluorogenic systems[22,51] our multi-wavelength probe additionally enables the read-out of more gates like INHIB (λ_{det} = 565-615 nm, Figure 2(g, h)) without further effort, thus providing additional information. The use of all four detection wavelengths enables distinction of each metabolization state and allows for sensitive multiparameter sensing. As physicians often evaluate clinical parameters by binary read-out to draw a first diagnosis, the range of different molecular logic gates qualifies our device for multipurpose use in medical diagnostics.[52] This is actually possible without further technical tools as color changes are visible even by the naked human eye. In summary these first preliminary tests hint to the use of **1** as a valuable tool for *live-cell* experiments, and other substrates with a broader application range are conceivable on the basis of scheme 1.

Fluorescent multi-wavelength pH-sensor **4**

Compound **4** contains two pH-sensitive groups which affect its spectral properties in a specific way (Figure 3(b) and 5, Table 3). The spectral variation is caused by the different emission of the photoacid (ROH) and corresponding base (RO^-) and by the change of the electron-withdrawing properties by protonation/deprotonation of the carboxylic acid group (σ_p ($R\text{-}CO_2H$) = 0.45[44]; σ_p ($R\text{-}CO_2^-$) = 0.00[44]). In contrast to compound **1**, where all the mutual combinations of substituents at the two orthogonal reaction sites are easily discernible (Figure 1(a, c)), only three states are visible in the emission spectra of **4** (Figure 3(a)). The assignment of protonation states of **4a-d** to the emissive species relies on similar spectroscopic features of compounds **1**-**3**, where the substituents exhibit similar Hammett-coefficients. Moreover, our interpretation also takes into account that the ordering of the acidities of the -OH and the -CO_2H group likely is reversed upon excitation due to the pronounced photoacidity of aromatic alcohols and the photobasicity of aromatic carboxylates.[53–56] This peculiarity leads to the situation that **4d** is the stable monovalent form in the ground state whereas isomeric **4b** is only found in the excited state. Förster-calculations to estimate lacking acidity constants e.g. of **4d** or **4b** are therefore not yet possible.

View Article Online
DOI: 10.1039/C6PP00290K

Figure 3

Table 3

At pH << 0, fluorescence emission of compound **4** at λ_{em} = 482 nm (Figure 3(b) and 5) results from the completely protonated excited species (**4a**). The excited-state acidity behind (pK_a*= -0.9) agrees well with the value of **2** (pK_a*,= -0.4; Table 1 and 3), evaluated by fluorescence titration (ESI S32, S30)[57,58], and also lies in the range of that of HPTA (N,N,N',N',N'',N''-hexamethyl-1,3,6-trisulfonamide) (pK_a* = -0.3).[43] Ongoing ESPT at pH values > 0 delivers the red shifted spectrum of the corresponding base (**4b**, λ_{em} = 557 nm). In this pH-range, i.e. 0 < pH < 4, no color change in the emission by conversion of **2** → **4** would be distinguishable because of the identical Hammett-coefficients of the -CO_2H and -CO_2Et substituents. At pH > 5, the fluorescence emission shifts hypsochromically due to deprotonation of the carboxylic acid thus reducing the electron-withdrawing strength (**4c**, λ_{em} = 536 nm). Please note, that the exact titration of the latter pK_a*-values using fluorescence intensities is hampered by convolution of the respective molar extinction coefficients with the ground state equilibria. Anyway, the two mentioned underlying pK_a*-values are experimentally accessible and are obtained from the trend of the depicted fluorescence titrations (Figure 3(a); see also ESI Figures S54, S55, S59, S60), whereas the pK_a*-values of the unstable isomeric form **4d** are not yet experimentally accessible.

Conventional absorption titration experiments allow for the determination of the ground state pK_a-values (ESI Figures S57, S58). Above pH 6.8, **4** is primarily present in the double deprotonated form (**4c**) and the excitation maximum shifts from λ_{ex} = 415 nm (**4d**) to λ_{ex} = 463 nm (**4c**, Table 3). The fluorescence intensity at λ_{det} = 548 nm therefore drops from pH 6.5 to 11 due to weak excitation with light of the wavelength λ_{ex} = 395 nm (Figure 5). A comparison with other pyrenol-derivatives provides insight into the electronic effects and supports our interpretation: structurally and electronically, **4** (as well as **2**) is a derivatives of the photoacid HPTA.[42,43,59–62] This molecule contains a third *N*,*N*'-dimethyl sulfonamide group (σ_p = 0.65) which is more electron-withdrawing than the carboxylate resp. the ester in dye **4d** and **2**. As the influence of σ_p is reflected in ground state acidity, the hydroxyl's pK_a of **2** and **4d** (pK_a = 6.6 and 6.8; Table 3) is about one logarithmic unit higher than that found for HPTA (pK_a = 5.6) but almost one unit below that of HPTS (8-Hydroxypyrene-1,3,6-trisulfonic acid).[43,63] It should be mentioned that the difference of hydroxyl's pK_a-values

View Article Online
DOI: 10.1039/C6PP00290K

between **2** and **4d** is less than expected, since the Hammett coefficients of the substituents (σ_p (R-CO_2Et) = 0.45; σ_p (R-CO_2^-) = 0.00) point to higher distinction. Indeed, the slightly lower pK_a-values obtained from FCS-experiments provide a larger difference (see ESI S37).

The second protonation equilibrium of **4a** due to deprotonation of the -CO_2H moiety is less clearly defined in the absorption spectra. Only a minor spectral shift between pH 0 and 3 from λ_{abs} = 418 to 415 nm (ESI Figure S56) prevents a reliable pK_a evaluation with absorption titration and provides only an estimate for the ground state pK_a-value of **4a**. Further experiments, including less ambiguous NMR-titrations with their demand for larger amounts of **4** and following the model by Ullmann[64], represent current research. Especially detection of the isomeric form **4b**, which appears to be less populated than in other systems[65], and the associated protonation equilibria in the electronic ground state deserve exhaustive investigations. It is, however, yet unclear whether the excited-state acidity constant of **4d** can be experimentally found by time-resolved spectroscopy.

As the pK_a and pK_a* of the hydroxyl and carboxyl group are significantly different and the prevalent protonation states can be identified via fluorescence and/or absorption spectroscopy, compound **4** can be used as optical sensor for a wide of range different pH values from highly acidic (pH < -1) to basic conditions (pH > 7). Four different pH-stages can be discriminated by optical spectroscopy due to the different spectral properties of species **4a**-**d**. While the pH values below -1 and between -0.5 and 4 resp. 5 and 6 can be identified via fluorescence spectroscopy, the pH-variation from 6 to 7 can be followed by a drop in fluorescence intensity (Figure 5). This idea can also be transferred to the concept of molecular logic.

Molecular logic

Although many examples of molecular logic are already known, we demonstrate the diversity of our systems which can act as different gates or mimic more complex operations. As each metabolization state of **1** is characterized by a distinct fluorescence color and thus several different output channels can be observed, probe **1** in combination with different enzyme inputs represents a versatile tool for molecular logic. This system is able to perform simple Boolean logic operations like AND (**O4**), NOR (**O1**) and INHIB (**O2**, **O3**) (Figure 4(a), Table 4, for details see ESI S50-S58). [27–29,66–68] Additionally, OR and XOR gates can be constructed by use of negative logic (see ESI S51, S57).[69] The logic gate which is mimicked by the system is determined by selection of a suitable output channel wavelength and threshold value. In any of the mentioned examples, a buffer solution of **1** without any enzyme is defined as initial state. By combination of several output channels and the two enzymes as input a 2:4

View Article Online
DOI: 10.1039/C6PP00290K

decoder[70–72], 1:2 demultiplexer[70,73,74], a half-adder[75–79] and -subtractor[69,78,79] and a transfer gate[70] (see ESI S49, S48, S59, S60, S56) can be implemented. Furthermore, a molecular keypad lock[70,80–86] is realized by use of acid phosphatase, potassium hydroxide and excitation light as input (see ESI S62).

Figure 4

To exemplify some logic operations, use of **1** as 2:4 decoder is explained in more detail. A 2:4 decoder translates binary information from two encoded (**In1**, **In2**) inputs to four unique outputs (**O1-O4**).[71] The truth table for this information processor is shown in Table 4. In the initial state, only **O1** is *on* due to the fluorescence emission of **1**. When either AlP (**In1**) or PLE (**In2**) is added, the substrate is converted into the corresponding product, which means that the substrate (**1**) fluorescence vanishes (**O1** = *off*) and solely the fluorescence of the formed dye is monitored (**O2** = *on* resp. **O4** = *on*). If both inputs are present, compound **4** is generated and the fluorescence at output channel **O4** exceeds the threshold value, while all other output channels are *off*.

Table 4

Reversible molecular logic was achieved with a Feynman gate (Figure 4(b, c), Table 4, see ESI S61). Here, **O5** represents the control output for the AlP input (YES-gate) and **O6** acts as XOR gate for AlP and PLE (target output). While the fluorescence emission at **O5** only exceeds the corresponding threshold value when AlP is present, simultaneous absence or presence of both PLE and AlP yields an emission at **O6** above the corresponding threshold. As output of **O6** is treated as negative logic, the XOR-like behavior is realized. The combination of these both gates to the Feynman gate generates a unique output pattern for each input.

Despite the presented system can process information in a logically reversible way, it is not resettable since **1** is irreversibly metabolized by the enzymes. Many resettable systems with a chelating motif use ions as input. However, resetting the system in its initial state usually requires removal of the ions with additional effort.[78,87] Alternative resettable systems use photons[70,71,81,88] or pH-variation as input.[77–79,89] In the latter case, H^+ and OH^- are used as inputs and the system becomes resettable, since these inputs can annihilate each other.[78]

Figure 5

View Article Online
DOI: 10.1039/C6PP00290K

In combination with definite amounts of H^+ and/or OH^- as input and a particular output wavelength, the pH-dependent fluorescence changes of **4** allow for mimicking nearly every simple logic operation (see ESI S63-S71). Moreover, the system can be applied as half-adder, half-subtractor and comparator[80,90] (see ESI S72-S74). In each of these applications, the system can be reset by addition of acid or base.

In the mentioned operation examples, the inputs are either chemically indistinguishable (same amounts of H^+ or OH^-) or can fully annihilate each other (same amounts of H^+ and OH^-). However, a reversible logic operation is achieved by choosing two different concentrations of base as input to create a Feynman gate (Figure 5, Table 5). While **O I** in the negative logic mode represents the YES gate for **In I** (low amount of OH^-), **O II** mimics a XOR gate for **In I** and **In II** (higher amount of OH^-). In the initial state at pH < 0, the emission above the threshold value at **O I** causes an *on*-response which is inverted by the negative operation to *off*. The same is true for the addition of **In II**, which sets the system to pH ~ 6.5. Each other scenario causes an *off* response which is converted to *on*. **O II** only processes an *on*-signal after **In I** or **In II** addition (pH ~ 3.5 or ~ 6.5, Figure 5, Table 5).

Conclusion and outlook

The dual enzyme probe **1** constitutes an efficient tool for monitoring orthogonal enzymatic activities producing four distinct emission colors which are distinguishable even by the naked human eye. It can act as individual probe for two different enzymes, allowing for their identification on basis of different fluorescence colors, and can as well indicate the presence of both enzymes. Internal referencing in a ratiometric way is enabled by the fluorescent substrate.

Compound **4** can be used as multi-wavelength sensor for a wide range of different pH values as the protonation states can be distinguished by their spectral properties. Furthermore, the two multi-wavelength ratiometric pyrene derivatives can be used for different applications of molecular logic. Beyond simple Boolean logic, both derivatives **1** and **4** are capable of more complex operations. Moreover, both systems can operate in a logically reversible way thus preventing information loss, and **4** can even be reset. Suchlike operation of **4** as non-trivial Feynman gate appears promising in view of our own attempts to combine chemistry with quantum optics.[91,92] The described synthesis allows for a modification of pyrenol into a multi-wavelength probe for other analytes or macromolecules. Since the color of the fluorescence emission strongly relies on the substitution of the hydroxyl group (position 6) by enabling or

View Article Online
DOI: 10.1039/C6PP00290K

disabling deprotonation and to a minor extent on the opposite position (position 1), more derivatives with orthogonal reactivities will be available. In summary, the described pyrenol derivatives present a versatile, flexible and chameleonic platform for the multianalyte probing and molecular logic in life science and chemistry.

Experimental section

UV/Vis and Fluorescence Spectroscopy

Absorption spectra were recorded with Jasco Spectrophotometer V-650, fluorescence emission and excitation spectra with Jasco Spectrofluorometer FP-6500. Concentrations of the measured solutions were in micromolar range if not stated otherwise.

Enzyme kinetics

All enzymatic *in vitro* reactions were examined at 25°C in aqueous buffer solution (0.1 M Tris-HCl at pH 8.0 for alkaline phosphatase (AlP) and porcine liver esterase (PLE); 0.1 M acetate at pH 5.0 for acid phosphatase (AP)). Esterase from porcine liver (activity = 18 units/mg solid) and acid phosphatase from potato (3.3 units/mg solid) were obtained as lyophilized powder from Sigma-Aldrich. Alkaline phosphatase from bovine intestinal mucosa in buffered aqueous solution (3.0 M NaCl, 0.2 mM $MgCl_2$, 30 mM triethanolamin, pH 7.6) with an activity of 3408 units/mg protein was also obtained from Sigma-Aldrich. Kinetic parameters were determined via fluorescence spectroscopy using a Lineweaver-Burk plot. Substrate concentrations were in the range of 0.1-25 μM and enzyme concentration was in the picomolar range in the case of AlP and in nanomolar range in that of PLE and AP. For determination of the kinetics, the decrease of the substrate fluorescence was monitored. When evolution of the product fluorescence is recorded, the observed kinetics were found to be nearly the same. Details can be found in the ESI S39-S45.

Two-photon excitation laser scanning microscopy

Laser scanning microscopy was performed with a confocal laser microscope (LSM510 META, Zeiss; Objective: Plan-Neofluar 40x/1.3, Zeiss). Excitation was performed with a Ti:Sa laser (Chameleon XR, Coherent) operating at $\lambda = 800$ nm.

Cell cultures

T 84 cells were grown in a 1:1 mixture of Ham's F12 medium and Dulbecco's modified Eagle's medium with 2.5 mM 95% L-glutamine and 5% fetal bovine serum before incubation

View Article Online
DOI: 10.1039/C6PP00290K

at 37°C, 5% CO_2 for 1-2 days. Before the experiment, the cells were washed with 0.25% (w/v) Trypsin- 0.53 mM EDTA solution to remove all traces of serum that contains trypsin inhibitor. L929 cells were grown in Eagle's Minimum Essential Medium modified to contain Earle's Balanced Salt Solution with non-essential amino acids, 2 mM L-glutamine, 1 mM sodium pyruvate, and 1500 mg/L sodium bicarbonate containing horse serum to a final concentration of 10% prior incubation at 37°C, 5% CO_2 for 1-2 days. Before the experiment, the cells were washed with 0.25% (w/v) Trypsin- 0.53 mM EDTA solution to remove all traces of serum that contains trypsin inhibitor. For incubation, compounds **1** and **3** were dissolved in water and dyes **2** and **4** were dissolved in DMSO.

Synthetic Procedures: General

All reagents and solvents were obtained from Sigma-Aldrich, Merck or Acros organics and used without further purification. For the chromatographic purification of compound **4**, Silica gel was washed prior to use with an 8:2 (v/v) mixture of methylene chloride / methanol and then dried in vacuo. Pyrenol was synthesized according to a modified procedure of Sehgal *et al*.[93]

^{1}H- and ^{13}C-NMR Spectra were recorded with a Bruker AM 400 spectrometer operating at 400 and 100 MHz, respectively. Alternatively, a Bruker AM 500 spectrometer operating at 500 *resp.* 125 MHz was used.

HRMS spectra were recorded with a Bruker solariX 7 Tesla instrument equipped with an Infinity Cell.

Data for X-Ray structure determination were collected on a X8 ApexII X-ray diffractometer operating with MoK/α radiation. Further details of the crystal data and structure refinement are gathered in Table S1 and S2 in the ESI.

6- and 8- bromopyren-1-ol (**5**). Pyrenol (120.0 mg, 0.55 mmol) was dissolved in absolute acetonitrile (20 mL) and cooled to -35°C. Subsequently, tetrafluoroboric acid diethyl ether complex (98.2 mg, 0.61 mmol) was introduced to the solution, and N-bromosuccinimide (107.6 mg, 0.61 mmol) was added in small portions. After stirring for 18 hours and warming to room temperature, the resultant black mixture was diluted with $NaHSO_3$ solution (38%, 30 mL) and stirred for additional 15 minutes. Diethylether (40 mL) was added and the resulting mixture was washed three times with water (40 mL) and once with saturated NaCl (40 mL) solution, before the organic phase was dried over sodium sulfate. After evaporation of the

View Article Online
DOI: 10.1039/C6PP00290K

solvent, the crude product was purified via column chromatography (diethylether/petrolether 40-65 = 4:6 (v/v)) and a mixture of 6- and 8-bromopyren-1-ol was obtained as white solid (142.0 mg, 0.48 mmol, 86%). UV/Vis (DMSO): λ_{max} = 358 nm, (DMSO+NaOH): λ_{max} = 472 nm; fluorescence (DMSO): λ_{max} = 399 nm, (DMSO+NaOH): λ_{max} = 477 nm. 6-bromopyren-1-ol: ^{1}H-NMR (400 MHz, acetone-d6, 25°C): δ = 9.68 (1H, s, OH), 8.58 (1 H, d, ^{3}J(H,H)= 9.6 Hz, Ar-*H*), 8.30 (1 H, d, ^{3}J(H,H) = 9.6 Hz, Ar-*H*), 8.22 – 8.14 (2 H, m, Ar-*H*), 8.05 – 8.01 (2 H, m, Ar-*H*), 7.88 (1 H, d, ^{3}J(H,H) = 9.0 Hz, Ar-*H*), 7.69 ppm (1 H, d, ^{3}J(H,H) = 8.5 Hz, Ar-*H*). ^{13}C-NMR (100 MHz, acetone-d6, 25°C): δ = 153.5, 132.6, 131.1, 131.0, 130.3, 128.9, 128.1, 127.2, 126.3, 125.8, 124.8, 124.7, 124.3, 119.5, 118.6, 114.8 ppm. 8-bromopyren-1-ol: ^{1}H-NMR (400 MHz, DMSO-d6, 25°C): δ = 9.67 (1H, s, OH), 8.48 (1 H, d, ^{3}J(H,H)= 9.3 Hz, Ar-*H*), 8.22 – 8.14 (4 H, m, Ar-*H*), 8.05 – 8.01 (2 H, m, Ar-*H*), 7.68 ppm (1 H, d, ^{3}J(H,H) = 8.3 Hz, Ar-*H*). ^{13}C-NMR (100 MHz, DMSO-d6, 25°C): δ = 153.7, 132.5, 131.1, 131.0, 127.8, 127.1, 126.4, 126.3, 125.6, 125.5, 125.4, 123.2, 122.8, 119.7, 118.9, 114.8 ppm. MS (ESI): *m/z* calc. for $C_{16}H_9BrO$: 294,975852 $[M-H]^-$, found: 294,97555.

3-bromo-8-hydroxy-*N*,*N*,*N'*,*N'*-tetramethylpyrene-1,6-disulfonamide and 3-bromo-6-hydroxy-*N*,*N*,*N'*,*N'*-tetramethylpyrene-1,8-disulfonamide (**6**). The mixture of regioisomers **5** (100.0 mg, 0.34 mmol) was dissolved in dry methylene chloride (20 mL) and cooled to -10°C. Chlorosulfonic acid (392.1 mg, 3.37 mmol) was added slowly and the resultant mixture was stirred for 18 hours upon warming up to room temperature. After addition of thionyl chloride (200.5 mg, 1.69mmol), the black slurry was heated to reflux for five hours. Before removal of the solvent and excessive thionyl chloride *in vacuo*, the resulting solution was cooled down to room temperature. After addition of dry THF (20 mL) to the residue and cooling to -10°C, dimethylamine dissolved in THF (1M, 10 mL) was added to the resulting solution. The reaction mixture was stirred for 18 hours, ethyl acetate was added and the organic phase was washed three times with hydrochloric acid (1M, 40 mL) and saturated NaCl solution (40 mL) before being dried over sodium sulfate. Subsequently, the solvent was evaporated and the crude product was purified by column chromatography (ethylacetate / petrolether 40-65 = 6:4 (v/v)) to yield the isomer mixture **6** (96.1 mg, 0.19 mmol, 56%) as yellow powder. UV/Vis (DMSO+TFA): λ_{max} = 432 nm, (DMSO): λ_{max} = 532 nm; fluorescence (DMSO; DMSO+TFA): λ_{max} = 450 nm, (DMSO): λ_{max} = 532 nm. 3-bromo-6-hydroxy-*N*,*N*,*N'*,*N'*-tetramethylpyrene-1,8-disulfonamide: ^{1}H-NMR (400 MHz, acetone-d6, 25°C): δ = 10.54 (1H, s, OH), 9.36 (1 H, d, ^{3}J (H,H) = 9.6 Hz, Ar-*H*), 9.23 (1 H, d, ^{3}J (H,H) = 9.6 Hz, Ar-*H*), 8.86 (1 H, s, Ar-*H*), 8.79 (1 H, d, ^{3}J (H,H) = 9.6 Hz, Ar-*H*), 8.50 (1 H, d, ^{3}J (H,H) = 9.6 Hz, Ar-*H*), 8.38 (1 H, s, Ar-*H*), 2.90 (6 H, s, 2 CH_3), 2.87 ppm (6 H, s, 2 CH_3).

View Article Online
DOI: 10.1039/C6PP00290K

^{13}C-NMR (100 MHz, acetone-d6, 25°C): δ = 153.9, 134.1, 133.8, 133.3, 131.5, 130.3, 129.4, 127.3, 126.8, 125.7, 125.1, 124.4, 122.7, 122.5, 119.5, 116.9, 38.1 (2C), 38.0 (2C) ppm. 3-bromo-8-hydroxy-*N*,*N*,*N'*,*N'*-tetramethylpyrene-1,6-disulfonamide: ^{1}H-NMR (400 MHz, acetone-d6, 25°C): δ = 10.54 (1H, s, OH), 9.27 (1 H, d, ^{3}J (H,H) = 10.0 Hz, Ar-*H*), 9.08 (1 H, d, ^{3}J (H,H) = 10.0 Hz, Ar-*H*), 8.86 (1 H, s, Ar-*H*), 8.85 (1 H, d, ^{3}J (H,H) = 9.6 Hz, Ar-*H*), 8.61 (1 H, d, ^{3}J (H,H) = 9.6 Hz, Ar-*H*), 8.38 (1 H, s, Ar-*H*), 2.91 (6 H, s, 2 CH_3), 2.88 ppm (6 H, s, 2 CH_3). ^{13}C-NMR (100 MHz, acetone-d6, 25°C): δ = 153.9, 134.6, 134.3, 133.9, 131.5, 133.4, 131.7, 129.3, 127.5, 127.3, 126.8, 126.5, 123.5, 122.1, 119.5, 116.9, 38.1 (2C), 38.0 (2C) ppm. MS (ESI): *m/z* calc. for $C_{20}H_{19}BrN_2O_5S_2$: 508,984052 $[M-H]^-$, found: 508,98384.

3-(benzyloxy)-8-bromo-*N*,*N*,*N'*,*N'*-tetramethylpyrene-1,6-disulfonamide (**7**). Sodium carbonate (329.4 mg, 2.28 mmol) and tetrabutylammonium iodide (TBAI) (17.2 mg, 0.05 mmol) were added to a solution of the isomer mix **6** (221.6 mg, 0.43 mmol) in dry acetone (50 mL). After addition of benzyl bromide (96.5 mg, 0.56 mmol), the orange solution was stirred for 42 hours at room temperature. The solvent was removed, methylene chloride (40 mL) was added and the organic phase was washed three times with hydrochloric acid (1M, 40 mL) and saturated NaCl solution (40 mL) before drying over sodium sulfate. Column chromatography (methylene chloride / petrolether 40-65 = 9:1 (v/v)) was used to purify the crude mixture of the resulting regioisomers and yielded **7** as yellow powder (116.7 mg, 0.19 mmol, 45 %). UV/Vis (DMSO): λ_{max} = 420 nm; fluorescence (DMSO): λ_{max} = 436 nm. ^{1}H-NMR (400 MHz, chloroform-d, 25°C): δ = 9.26 (1 H, d, ^{3}J (H,H) = 9.8 Hz), 9.27 (1 H, d, ^{3}J (H,H) = 9.19 Hz, Ar-*H*), 8.93 (1 H, s, Ar-*H*), 8.82 (1 H, d, ^{3}J (H,H) = 9.8 Hz, Ar-*H*), 8.49 (1 H, d, ^{3}J (H,H) = 9.8 Hz, Ar-*H*), 8.32 (1 H, s, Ar-*H*), 7.5 (5 H, m, Ar-*H*), 5,58 (2 H, s, CH_2), 2.89 (6 H, s, 2 CH_3), 2.72 ppm (6 H, s, 2 CH_3). ^{13}C-NMR (100 MHz, chloroform-d, 25°C): δ = 152.8, 135.8, 132.9, 132.8, 131.8, 130.6, 128.9 (2 C), 128.8, 128.5, 127.9, 127.5 (3C), 126.2, 125.6, 125.4, 123.5, 123.3, 122.7, 119.8, 112.9, 71.3, 37.6 (2C), 37.5 (2C) ppm. MS (ESI): *m/z* calc. for $C_{27}H_{25}BrN_2O_5S_2$: 623,028043 $[M+Na]^+$, found: 623,02891.

Ethyl 6-(benzyloxy)-3,8-bis(*N*,*N*-dimethylsulfamoyl)pyrene-1-carboxylate (**8**). Compound **7** (64.5 mg, 0.11 mmol) was dissolved in a reaction tube with a mixture of benzene (9.29 mL), triethyamine (3.44 mL) and ethanol (1.82 mL). Before the tube was introduced in the autoclave, $[Pd(PPh_3)_2Cl_2]$ was added to the reaction mixture which then was heated to 65°C for 12 hours under a CO pressure of 16 bar. The solution was cooled the room temperature and transferred to a 100 mL flask, the solvent was removed and the residue was dissolved in methylene chloride (30 mL). Before being dried over sodium sulfate and evaporation of the

View Article Online
DOI: 10.1039/C6PP00290K

solvent, the organic phase was washed three times with water (30 mL) and saturated NaCl solution (30 mL). Compound **8** was obtained as yellow powder after column chromatography (methylene chloride / petrolether 40-65 = 9:1 (v/v)) in a yield of 80% (48.9 mg, 0.09 mmol). UV/Vis (DMSO): λ_{max} = 420 nm; fluorescence (DMSO): λ_{max} = 462 nm. ^{1}H-NMR (400 MHz, chloroform-d, 25°C): δ = 9.24 (4 H, m, Ar-*H*), 8.91 (1 H, ^3J (H,H) = 9.6 Hz Ar-*H*), 8.32 (1 H, s, Ar-*H*), 7.47 ppm (5 H, m, Ar-*H*), 5,59 (2 H, s, CH_2), 4,61 (2H, q, ^3J (H,H) = 7.3 Hz, CH_2) 2.90 (6 H, s, 2 CH_3), 2.73 (6 H, s, 2 CH_3), 1,55 ppm (3H, t, ^3J (H,H) = 7.3 Hz, CH_3). ^{13}C-NMR (100 MHz, chloroform-d, 25°C): δ = 166.6, 153.2, 135.7, 135.0, 133.9, 132.5, 131.9, 131.1, 130.5, 129.5, 128.9, 128.5, 128.0, 127.5, 125.8, 125.7, 125.2, 125.0, 124.2, 123.9, 123.2, 122.1, 112.7, 71.3, 62.0, 37.5 (4C), 14.4 ppm. MS (ESI): *m/z* calc. for $C_{30}H_{30}N_2O_7S_2$: 617,138661 $[M+Na]^+$, found: 617,13953.

Ethyl 3,8-bis(*N*,*N*-dimethylsulfamoyl)-6-hydroxypyrene-1-carboxylate (**2**). In a 100 mL flask equipped with reflux condenser and a gas bubbler, ammonium formate (223.4 mg, 63.1 mmol) and palladium on carbon (10% w/t, 360 mg) were added to a solution of **8** (202.2 mg, 0.35 mmol) in acetone (40 mL). The reaction suspension was heated to reflux. When the evolution of gas ceased, the mixture was stirred for an additional hour. After cooling to room temperature, the suspension was filtered through a plug of celite and the solvent of the resulting solution was evaporated. The residue was dissolved in ethyl acetate (40 mL), washed three times with hydrochloric acid (1M, 40 mL) and saturated NaCl solution (40 mL) and dried over sodium sulfate. Column chromatography (ethylacetate / petrolether 40-65 = 6:4 (v/v)) of the raw product yielded **2** as yellow powder (143.0 mg, 0.30 mmol, 85%). UV/Vis (DMSO+TFA): λ_{max} = 426 nm, (DMSO): λ_{max} = 559 nm, (H_2O+HCl): λ_{max} = 419 nm, (H_2O): λ_{max} = 494 nm; ; $\varepsilon_{(494)}$ (H_2O, RO^-) = 25000 L mol^{-1} cm^{-1}; fluorescence (DMSO+TFA): λ_{max} = 482/576 nm, (DMSO): λ_{max} = 576 nm, (H_2O+HCl): λ_{max} = 478 nm, (H_2O): λ_{max} = 558 nm. ^{1}H-NMR (500 MHz, acetone-d6, 25°C): δ = 9.34 (1 H, d, ^3J (H,H) = 10.0 Hz, Ar-*H*), 9.28 (1 H, d, ^3J (H,H) = 9.4 Hz, Ar-*H*), 9.25 (1 H, ^3J (H,H) = 10.0 Hz Ar-*H*), 9.21 (1 H, s, Ar-*H*), 8.88 (1 H, d, ^3J (H,H) = 9.4 Hz, Ar-*H*), 8.38 (1 H, s, Ar-*H*), 4,60 (2H, q, ^3J (H,H) = 7.3 Hz, CH_2), 2.89 (6 H, s, 2 CH_3), 2.88 (6 H, s, 2 CH_3), 1,53 ppm (3H, t, ^3J (H,H) = 7.3 Hz, CH_3). ^{13}C-NMR (125 MHz, acetone-d6, 25°C): δ = 167.3, 154.3, 134.7 (2C), 132.2, 131.8, 130.4, 129.2, 127.1, 126.8, 126.0, 125.6, 124.6, 124.0, 122.4, 122.1, 116.8, 62.6, 38.1 (2C), 38.0 (2C), 14.8 ppm. MS (ESI): *m/z* calc. for $C_{23}H_{24}N_2O_7S_2$: 503,09467 $[M-H]^-$, found: 503,09282.

3,8-bis(N,N-dimethylsulfamoyl)-6-hydroxypyrene-1-carboxylic acid (**4**). Compound **2** (17.8 mg, 0.04 mmol) was dissolved in dry THF (10 mL) to which was then added water

View Article Online
DOI: 10.1039/C6PP00290K

(3.06 mg, 0.17 mmol) and potassium *tert*-butoxide (83.04 mg, 0.74 mmol). The reaction mixture was stirred 24 hours at room temperature, before the addition of ethyl acetate (20 mL). Subsequently, the organic phase was washed three times with hydrochloric acid (1M, 20 mL) and saturated NaCl solution (20 mL) and dried over sodium sulfate. **4** was purified with column chromatography (methylene chloride / methanol = 9:1 (v/v)) to give a yellow powder (12.6 mg, 0.03 mmol, 72%). UV/Vis (DMSO+TFA): λ_{max} = 425 nm, (DMSO): λ_{max} = 424/557 nm, (H_2O+HCl): λ_{max} = 415/418 nm, (H_2O): λ_{max} = 463 nm; $\varepsilon_{(463)}$ (H_2O, RO^-) = 17000 L mol^{-1} cm^{-1}; fluorescence (DMSO+TFA): λ_{max} = 476/573 nm, (DMSO): λ_{max} = 573 nm, (H_2O+HCl): λ_{max} = 482 nm, (H_2O): λ_{max} = 536/557 nm. ^{1}H-NMR (500 MHz, acetone-d6, 25°C): δ = 9.38 (1 H, d, ^3J (H,H) = 10.0 Hz, Ar-*H*), 9.24 (1 H, d, ^3J (H,H) = 9.6 Hz, Ar-*H*), 9.20 (1 H, ^3J (H,H) = 10.0 Hz Ar-*H*), 9.16 (1 H, s, Ar-*H*), 8.79 (1 H, d, ^3J (H,H) = 9.6 Hz, Ar-*H*), 8.34 (1 H, s, Ar-*H*), 2.88 (6 H, s, 2 CH_3), 2.85 ppm (6 H, s, 2 CH_3). ^{13}C-NMR (125 MHz, acetone-d6, 25°C): δ = 179.3, 153.8, 134.1, 133.7, 132,1, 131.7, 130.0, 128.8, 127.9, 127.2, 126.0, 125.6, 125.4, 125.0, 122.4, 122.2, 116.3, 38.1 (2C), 38.0 (C2). MS (ESI): *m/z* calc. for $C_{21}H_{20}N_2O_7S_2$: 475,06337 $[M-H]^-$, found: 475,06494.

Ethyl 3,8-bis(*N*,*N*-dimethylsulfamoyl)-6-(phosphonooxy)pyrene-1-carboxylate (**1**). After dissolving phosphoroxy chloride (140 µL) in dry methylene chloride (40 mL) and cooling to -10°C, a solution of **2** (48.1 mg, 0.10 mmol) and trimethylamine (40 µL) in dry methylene chloride (20 mL) was added slowly. The resulting, nearly colorless, solution was stirred for 18 hours upon warming up slowly to room temperature. Water (3 mL) was added slowly and the mixture was stirred for additional 10 minutes. The organic phase was washed three times with cooled water (~5°C, 40 mL) and one time with saturated NaCl solution (~5°C, 40 mL) before drying over sodium sulfate. After evaporation of the solvent, the raw dichlorophosphate was dissolved in a mixture of water (5 mL) and acetone (5 mL). Hydrolysis was monitored by RP-TLC and was complete after 48 hours. The reaction mixture was extracted three times with ethyl acetate and the aqueous phase was dried *in vacuo*. Reverse phase column chromatography (water / methanol = 1:1 (v/v)) of the crude product yielded **1** as yellow powder (37.6 mg, 0.07 mmol, 68%). UV/Vis (H_2O): λ_{max} = 410 nm; $\varepsilon_{(410)}$ (H_2O) = 19300 L mol^{-1} cm^{-1}; fluorescence (H_2O): λ_{max} = 472 nm. ^{1}H-NMR (500 MHz, methanol-d4, 25°C): δ = 9.35 (1 H, d, ^3J (H,H) = 10.0 Hz, Ar-*H*), 9.30 (1 H, d, ^3J (H,H) = 9.6 Hz, Ar-*H*), 9.24 (1 H, ^3J (H,H) = 10.0 Hz Ar-*H*), 9.19 (1 H, s, Ar-*H*), 8.92 (1 H, d, ^3J (H,H) = 10.0 Hz, Ar-*H*), 8.86 (1 H, s, Ar-*H*), 4.61 (2H, q, ^3J (H,H) = 7.0 Hz, CH_2), 2.93 (6 H, s, 2 CH_3), 2.86 (6 H, s, 2 CH_3), 1,55 ppm (3H, t, ^3J (H,H) = 7.0 Hz, CH_3). ^{13}C-NMR (125 MHz, methanol-d4, 25°C): δ = 168.0, 150.2, 134.9, 134.7, 133.3, 132.1, 131.1, 129.4, 127.1, 127.0, 126.9, 126.6, 125.8,

View Article Online
DOI: 10.1039/C6PP00290K

125.5, 124.9, 121.3 (C2), 63.3, 38.4 (C2), 38.0 (C2), 14.9 ppm. MS (ESI): *m/z* calc. for $C_{23}H_{25}N_2O_{10}PS_2$: 583,06155 $[M-H]^-$, found: 583,06245.

3,8-bis(*N*,*N*-dimethylsulfamoyl)-6-(phosphonooxy)pyrene-1-carboxylic acid (**3**). Compound **1** (4.0 mg, 0.007) was dissolved in an aqueous solution of NaOH (0.05 M, 10 mL). Reaction progress was monitored with RP-TLC and found to be complete after 2 hours. The pH of the reaction solution was neutralized, and the water was evaporated from the aqueous phase after extraction with ethyl acetate. The crude product was purified by reverse phase column chromatography (water / methanol = 7:3 (v/v)) and yielded **3** as yellow powder (3.1 mg, 0.006 mmol, 81%). UV/Vis (H_2O): λ_{max} = 407 nm; $\varepsilon_{(407)}$ (H_2O) = 15000 L mol^{-1} cm^{-1}; fluorescence (H_2O): λ_{max} = 448 nm. ^{1}H-NMR (500 MHz, methanol-d4, 25°C): δ = 9.25 (1 H, d, ^3J (H,H) = 9.8 Hz, Ar-*H*), 9.24 (1 H, d, ^3J (H,H) = 9.8 Hz, Ar-*H*), 8.97 (1 H, ^3J (H,H) = 10.0 Hz Ar-*H*), 8.89 (1 H, s, Ar-*H*), 8.87 (1 H, s, Ar-*H*), 8.86 (1 H, d, ^3J (H,H) = 10.0 Hz, Ar-*H*), 2.90 (6 H, s, 2 CH_3), 2.86 ppm (6 H, s, 2 CH_3). ^{13}C-NMR (125 MHz, methanol-d4, 25°C): δ = 175.5, 149.7, 136.9, 133.1, 132.4, 130.9, 130.7, 129.8, 127.6, 127.5, 127.1, 127.0, 126.8, 126.7, 125.4, 125.3, 121.1, 38.4 (C2), 38.1 (C2) ppm. MS (ESI): *m/z* calc. for $C_{21}H_{21}N_2O_{10}PS_2$: 555,03025 $[M-H]^-$, found: 555,03196.

Acknowledgements

Financial support by the German Science Foundation (DFG, JU650/7-1) is gratefully noticed. Furthermore we thank Tobias Dier for recording the mass spectra, Volker Huch for X-ray crystallography measurements and Alexander Schiller for the helpful discussion of our manuscript.

Electronic Supplementary Information (ESI)

Further compound characterization, determination of enzyme kinetics, further preliminary *live-cell* experiments and details for molecular logic are provided in the *Electronic Supplementary Information* (ESI).

View Article Online
DOI: 10.1039/C6PP00290K

Notes and references

1. Baruch, A., Jeffery, D. A. & Bogyo, M. 2004 Enzyme activity – it's all about image. *Trends Cell Biol.* **14**, 29–35.

2. Kikuchi, K. 2010 Design, synthesis and biological application of chemical probes for bio-imaging. *Chem. Soc. Rev.* **39**, 2048–2053.

3. Lee, M. H., Kim, J. S. & Sessler, J. L. 2015 Small molecule-based ratiometric fluorescence probes for cations, anions, and biomolecules. *Chem. Soc. Rev.* **44**, 4185–4191.

4. Lakowicz, J. R. 2006 *Principles of Fluorescence Spectroscopy*. 3rd edn. Springer.

5. Johnson, I. & Spence, M. T. Z. 2010 *The Molecular Probes Handbook*.

6. Li, X., Gao, X., Shi, W. & Ma, H. 2014 Design strategies for water-soluble small molecular chromogenic and fluorogenic probes. *Chem. Rev.* **114**, 590–659.

7. Yee, D. J., Balsanek, V., Bauman, D. R., Penning, T. M. & Sames, D. 2006 Fluorogenic metabolic probes for direct activity readout of redox enzymes: Selective measurement of human AKR1C2 in living cells. *Proc. Natl. Acad. Sci. U. S. A.* **103**, 13304–13309.

8. Shi, H., Kwok, R. T. K., Liu, J., Xing, B., Tang, B. Z. & Liu, B. 2012 Real-time monitoring of cell apoptosis and drug screening using fluorescent light-up probe with aggregation-induced emission characteristics. *J. Am. Chem. Soc.* **134**, 17972–17981.

9. Kamiya, M., Asanuma, D., Kuranaga, E., Takeishi, A., Sakabe, M., Miura, M., Nagano, T. & Urano, Y. 2011 β-galactosidase fluorescence probe with improved cellular accumulation based on a spirocyclized rhodol scaffold. *J. Am. Chem. Soc.* **133**, 12960–12963.

10. Demchenko, A. P. 2014 Practical aspects of wavelength ratiometry in the studies of intermolecular interactions. *J. Mol. Struct.* **1077**, 51–67.

11. Demchenko, A. P. 2010 The concept of λ-ratiometry in fluorescence sensing and imaging. *J. Fluoresc.* **20**, 1099–1128.

12. Liu, Z.-M., Feng, L., Ge, G.-B., Lv, X., Hou, J., Cao, Y.-F., Cui, J.-N. & Yang, L. 2014 A highly selective ratiometric fluorescent probe for in vitro monitoring and cellular imaging of human carboxylesterase 1. *Biosens. Bioelectron.* **57**, 30–35.

13. Song, Z., Kwok, R. T. K., Zhao, E., He, Z., Hong, Y., Lam, J. W. Y., Liu, B. & Tang, B. Z. 2014 A ratiometric fluorescent probe based on ESIPT and AIE processes for alkaline phosphatase activity assay and visualization in living cells. *ACS Appl. Mater. Interfaces* **6**, 17245–17254.

14. Kurishita, Y., Kohira, T., Ojida, A. & Hamachi, I. 2010 Rational design of FRET-based ratiometric chemosensors for in vitro and in cell fluorescence analyses of nucleoside polyphosphates. *J. Am. Chem. Soc.* **132**, 13290–13299.

View Article Online
DOI: 10.1039/C6PP00290K

15. Chen, L. et al. 2013 The first ratiometric fluorescent probes for aminopeptidase N cell imaging. *Org. Biomol. Chem.* **11**, 378–382.

16. Komatsu, T., Urano, Y., Fujikawa, Y., Kobayashi, T., Kojima, H., Terai, T., Hanaoka, K. & Nagano, T. 2009 Development of 2,6-carboxy-substituted boron dipyrromethene (BODIPY) as a novel scaffold of ratiometric fluorescent probes for live cell imaging. *Chem. Commun.*, 7015–7017.

17. Debieu, S. & Romieu, A. 2015 Dual enzyme-responsive 'turn-on' fluorescence sensing systems based on in situ formation of 7-hydroxy-2-iminocoumarin scaffolds. *Org. Biomol. Chem.* **13**, 10348–10361.

18. Halámek, J. et al. 2010 Multiplexing of injury codes for the parallel operation of enzyme logic gates. *Analyst* **135**, 2249–2259.

19. Halámková, L., Halámek, J., Bocharova, V., Wolf, S., Mulier, K. E., Beilman, G., Wang, J. & Katz, E. 2012 Analysis of biomarkers characteristic of porcine liver injury--from biomolecular logic gates to an animal model. *Analyst* **137**, 1768–1770.

20. Romieu, A. 2015 'AND' luminescent 'reactive' molecular logic gates: a gateway to multi-analyte bioimaging and biosensing. *Org. Biomol. Chem.* **13**, 1294–1306.

21. Li, Y., Wang, H., Li, J., Zheng, J., Xu, X. & Yang, R. 2011 Simultaneous intracellular β-D-glucosidase and phosphodiesterase I activities measurements based on a triple-signaling fluorescent probe. *Anal. Chem.* **83**, 1268–1274.

22. Prost, M. & Hasserodt, J. 2014 'Double gating' - a concept for enzyme-responsive imaging probes aiming at high tissue specificity. *Chem. Commun.* **50**, 14896–14899.

23. Li, S.-Y., Liu, L.-H., Cheng, H., Li, B., Qiu, W.-X. & Zhang, X.-Z. 2015 A dual-FRET-based fluorescence probe for the sequential detection of MMP-2 and caspase-3. *Chem. Commun.* **51**, 14520–14523.

24. Kim, T.-I., Kim, H., Choi, Y. & Kim, Y. 2011 A fluorescent turn-on probe for the detection of alkaline phosphatase activity in living cells. *Chem. Commun.* **47**, 9825–9827.

25. Millán, J. L. & Fishman, W. H. 1995 Biology of human alkaline phosphatases with special reference to cancer. *Crit. Rev. Clin. Lab. Sci.* **32**, 1–39.

26. Zhang, Y., Chen, W., Feng, D., Shi, W., Li, X. & Ma, H. 2012 A spectroscopic off-on probe for simple and sensitive detection of carboxylesterase activity and its application to cell imaging. *Analyst* **137**, 716–721.

27. Andréasson, J. & Pischel, U. 2015 Molecules with a sense of logic: a progress report. *Chem. Soc. Rev.* , 1053–1069.

28. de Silva, A. P. 2013 *Molecular logic-based computation*. RSC Publishing.

29. Szaciłowski, K. 2012 *Infochemistry: Information Processing at the Nanoscale*. WILEY-VCH.

30. Gassman, P. & Schenk, W. 1977 A general procedure for the base-promoted hydrolysis of hindered esters at ambient temperatures. *J. Org. Chem.* **42**, 918–920.

31. Förster, T. 1950 Elektrolytische Dissoziation angeregter Moleküle. *Zeitschrift für*

View Article Online
DOI: 10.1039/C6PP00290K

Elektrochemie **54**, 42–46.

32. Pines, E. 2003 *The Chemistry of Phenols*. John Wiley & Sons Ltd.
33. Agmon, N. 2005 Elementary steps in excited-state proton transfer. *J. Phys. Chem. A* **109**, 13–35.
34. Tolbert, L. M. & Haubrich, J. E. 1990 Enhanced photoacidities of cyanonaphthols. *J. Am. Chem. Soc.* **112**, 8163–8165.
35. Tolbert, L. M. & Haubrich, J. E. 1994 Photoexcited proton transfer from enhanced photoacids. *J. Am. Chem. Soc.* **116**, 10593–10600.
36. Huppert, D., Tolbert, L. M. & Linares-Samaniego, S. 1997 Ultrafast excited-state proton transfer from cyano-substituted 2-naphthols. *J. Phys. Chem. A* **101**, 4602–4605.
37. Clower, C., Solntsev, K. M., Kowalik, J., Tolbert, L. M. & Huppert, D. 2002 Photochemistry of ' super ' photoacids . 3 . excited-state proton transfer from perfluoroalkylsulfonyl-substituted 2-naphthols. *J. Phys. Chem. A* **106**, 3114–3122.
38. Tran-Thi, T.-H., Prayer, C., Millié, P., Uznanski, P. & Hynes, J. T. 2002 Substituent and solvent effects on the nature of the transitions of pyrenol and pyranine. identification of an intermediate in the excited-state proton-transfer reaction. *J. Phys. Chem. A* **106**, 2244–2255.
39. Solntsev, K. M., Sullivan, E. N., Tolbert, L. M., Ashkenazi, S., Leiderman, P. & Huppert, D. 2004 Excited-state proton transfer reactions of 10-hydroxycamptothecin. *J. Am. Chem. Soc.* **126**, 12701–12708.
40. Prémont-Schwarz, M., Barak, T., Pines, D., Nibbering, E. T. J. & Pines, E. 2013 Ultrafast excited state proton transfer reaction of 1-naphthol-3,6-disulfonate and several 5-substituted 1-naphthol derivatives. *J. Phys. Chem. B* **117**, 4593–4594.
41. Spies, C., Finkler, B., Acar, N. & Jung, G. 2013 Solvatochromism of pyranine-derived photoacids. *Phys. Chem. Chem. Phys.* **15**, 19893–19905.
42. Spies, C., Shomer, S., Finkler, B., Pines, D., Pines, E., Jung, G. & Huppert, D. 2014 Solvent dependence of excited-state proton transfer from pyranine-derived photoacids. *Phys. Chem. Chem. Phys.* **16**, 9104–9114.
43. Finkler, B. et al. 2014 Highly photostable 'super'-photoacids for ultrasensitive fluorescence spectroscopy. *Photochem. Photobiol. Sci.* **13**, 548–562.
44. Hansch, C., Leo, A. & Taft, R. W. 1991 A survey of hammett substituent constants and resonance and field parameters. *Chem. Rev.* **91**, 165–195.
45. Fernley, H. N. & Walker, P. G. 1965 Kinetic behaviour of calf-intestinal alkaline phosphatase with 4-methylumbelliferyl phosphate. *Biochem. J.* **97**, 95–103.
46. Lun, S. & Bishai, W. R. 2007 Characterization of a novel cell wall-anchored protein with carboxylesterase activity required for virulence in mycobacterium tuberculosis. *J. Biol. Chem.* **282**, 18348–18356.
47. Provencher, L. & Jones, J. B. 1994 A concluding specification of the dimensions of the active site model of pig liver esterase. *J. Org. Chem.* **59**, 2729–2732.
48. De María, P. D., García-Burgos, C. A., Bargeman, G. & Van Gemert, R. W. 2007 Pig liver esterase (PLE) as biocatalyst in organic synthesis: From nature to cloning and to practical applications. *Synthesis.* **10**, 1439–1452.

View Article Online
DOI: 10.1039/C6PP00290K

49. Ward, J. L. & Tse, C. M. 1999 Nucleoside transport in human colonic epithelial cell lines: evidence for two Na^+-independent transport systems in T84 and Caco-2 cells. *Biochim. Biophys. Acta Biomembr.* **1419**, 15–22.

50. Pastor-Anglada, M., Cano-Soldado, P., Molina-Arcas, M., Lostao, M. P., Larráyoz, I., Martínez-Picado, J. & Casado, F. J. 2005 Cell entry and export of nucleoside analogues. *Virus Res.* **107**, 151–164.

51. Win, M. N. & Smolke, C. D. 2008 Higher-order cellular information processing with synthetic RNA devices. *Science* **322**, 456–460.

52. Elstner, M., Axthelm, J. & Schiller, A. 2014 Sugar-based molecular computing by material implication. *Angew. Chemie Int. Ed.* **53**, 7339–7343.

53. Ditkovich, J., Mukra, T., Pines, D., Huppert, D. & Pines, E. 2015 Bifunctional photoacids: Remote protonation affecting chemical reactivity. *J. Phys. Chem. B* **119**, 2690–2701.

54. Zelent, B., Vanderkooi, J. M., Coleman, R. G., Gryczynski, I. & Gryczynski, Z. 2006 Protonation of excited state pyrene-1-carboxylate by phosphate and organic acids in aqueous solution studied by fluorescence spectroscopy. *Biophys. J.* **91**, 3864–3871.

55. Nucci, N. V., Zelent, B. & Vanderkooi, J. M. 2008 Pyrene-1-carboxylate in water and glycerol solutions: Origin of the change of pK upon excitation. *J. Fluoresc.* **18**, 41–49.

56. Zelent, B., Vanderkooi, J. M., Nucci, N. V., Gryczynski, I. & Gryczynski, Z. 2009 Phosphate assisted proton transfer in water and sugar glasses: A study using fluorescence of pyrene-1-carboxylate and IR spectroscopy. *J. Fluoresc.* **19**, 21–31.

57. Weller, A. 1959 Outer and inner mechanism of reactions of excited molecules. *Discuss. Faraday Soc.* **27**, 28–33

58. Weller, A. 1961 Fast reactions of excited molecules. *Progrogress React. Kinet.* **1**, 187–214.

59. Spry, D. B. & Fayer, M. D. 2007 Observation of slow charge redistribution preceding excited-state proton transfer. *J. Chem. Phys.* **127**, 204501.

60. Pines, E., Pines, D., Ma, Y.-Z. & Fleming, G. R. 2004 Femtosecond pump-probe measurements of solvation by hydrogen-bonding interactions. *ChemPhysChem* **5**, 1315–1327.

61. Spry, D. B. & Fayer, M. D. 2007 Observation of slow charge redistribution preceding excited-state proton transfer. *J. Chem. Phys.* **127**, 204501 1-10.

62. Spies, C., Finkler, B., Acar, N. & Jung, G. 2013 Solvatochromism of pyranine-derived photoacids. *Phys. Chem. Chem. Physic* **15**, 19893–19905.

63. Offenbacher, H., Wolfbeis, O. S. & Furlinger, E. 1986 Fluorescence optical sensors for continuous determination of near-neutral pH values. *Sensors and Actuators* **9**, 73–84.

64. Ullmann, G. M. 2003 Relations between protonation constants and titration curves in polyprotic acids: A critical view. *J. Phys. Chem. B* **107**, 1263–1271.

65. Bizzarri, R. et al. 2007 Green fluorescent protein ground states: The influence of a second protonation site near the chromophore. *Biochemistry* **46**, 5494–5504.

66. de Silva, A. P., Gunaratne, N. H. Q. & McCoy, C. P. 1993 A molecular photoionic

View Article Online
DOI: 10.1039/C6PP00290K

AND gate based on fluorescent signalling. *Nature* **364**, 42–44.

67. Andréasson, J. & Pischel, U. 2010 Smart molecules at work-mimicking advanced logic operations. *Chem. Soc. Rev.* **39**, 174–188.

68. de Silva, A. P. & McClenaghan, N. D. 2004 Molecular-scale logic gates. *Chem. - An Eur. J.* **10**, 574–586.

69. Coskun, A., Deniz, E. & Akkaya, E. U. 2005 Effective PET and ICT switching of boradiazaindacene emission: A unimolecular, emission-mode, molecular half-subtractor with reconfigurable logic gates. *Org. Lett.* **7**, 5187–5189.

70. Andréasson, J., Pischel, U., Straight, S. D., Moore, T. a, Moore, A. L. & Gust, D. 2011 All-photonic multifunctional molecular logic device. *J. Am. Chem. Soc.* **133**, 11641–11648.

71. Andréasson, J., Straight, S. D., Moore, T. A., Moore, A. L. & Gust, D. 2008 Molecular all-photonic encoder-decoder. *J. Am. Chem. Soc.* **130**, 11122–11128.

72. Kang, D., White, R. J., Xia, F., Zuo, X., Vallée-Bélisle, A. & Plaxco, K. W. 2012 DNA biomolecular-electronic encoder and decoder devices constructed by multiplex biosensors. *NPG Asia Mater.* **4**, e1.

73. Orbach, R., Remacle, F., Levine, R. D. & Willner, I. 2014 DNAzyme-based 2:1 and 4:1 multiplexers and 1:2 demultiplexer. *Chem. Sci.* **5**, 1074–1081.

74. Zhao, L., Xia, W. & Yang, C. 2014 Fluorescent 1:2 demultiplexer and half-subtractor based on the hydrolysis of N-salicylidene-3-aminopyridine. *Spectrochim. Acta. A. Mol. Biomol. Spectrosc.* **117**, 397–401.

75. Andréasson, J., Kodis, G., Terazono, Y., Liddell, P. A., Bandyopadhyay, S., Mitchell, R. H., Moore, T. A., Moore, A. L. & Gust, D. 2004 Molecule-based photonically switched half-adder. *J. Am. Chem. Soc.* **126**, 15926–15927.

76. Remacle, F., Weinkauf, R. & Levine, R. D. 2006 Molecule-based photonically switched half and full adder. *J. Phys. Chem. A* **110**, 177–184.

77. Pei, H., Liang, L., Yao, G., Li, J., Huang, Q. & Fan, C. 2012 Reconfigurable three-dimensional DNA nanostructures for the construction of intracellular logic sensors. *Angew. Chemie Int. Ed.* **51**, 9020–9024.

78. Margulies, D., Melman, G. & Shanzer, A. 2005 Fluorescein as a model molecular calculator with reset capability. *Nat. Mater.* **4**, 768–771.

79. Margulies, D., Melman, G. & Shanzer, A. 2006 A molecular full-adder and full-subtractor, an additional step toward a moleculator. *J. Am. Chem. Soc.* **128**, 4865–4871.

80. Margulies, D., Felder, C. E., Melman, G. & Shanzer, A. 2007 A molecular keypad lock: A photochemical device capable of authorizing password entries. *J. Am. Chem. Soc.* **129**, 347–354.

81. Remón, P., Hammarson, M., Li, S., Kahnt, A., Pischel, U. & Andréasson, J. 2011 Molecular implementation of sequential and reversible logic through photochromic energy transfer switching. *Chem. - An Eur. J.* **17**, 6492–6500.

82. Li, Q., Yue, Y., Guo, Y. & Shao, S. 2012 Fluoride anions triggered 'OFF–ON' fluorescent sensor for hydrogen sulfate anions based on a BODIPY scaffold that works

View Article Online
DOI: 10.1039/C6PP00290K

as a molecular keypad lock. *Sensors Actuators B Chem.* **173**, 797–801.

83. Jiang, X.-J. & Ng, D. K. P. 2014 Sequential logic operations with a molecular keypad lock with four inputs and dual fluorescence outputs. *Angew. Chemie Int. Ed.* **53**, 10481–10484.

84. Rout, B., Milko, P., Iron, M. A., Motiei, L. & Margulies, D. 2013 Authorizing multiple chemical passwords by a combinatorial molecular keypad lock. *J. Am. Chem. Soc.* **135**, 15330–15333.

85. Strack, G., Ornatska, M., Pita, M. & Katz, E. 2008 Biocomputing security system: concatenated enzyme-based logic gates operating as a biomolecular keypad lock. *J. Am. Chem. Soc.* **130**, 4234–5235.

86. Chen, J., Zhou, S. & Wen, J. 2014 Concatenated logic circuits based on a three-way DNA junction: A keypad-lock security system with visible readout and an automatic reset function. *Angew. Chemie Int. Ed.* **54**, 446–450.

87. De Silva, A. P. & McClenaghan, N. D. 2000 Proof-of-principle of molecular-scale arithmetic. *J. Am. Chem. Soc.* **122**, 3965–3966.

88. Remón, P., Bälter, M., Li, S., Andréasson, J. & Pischel, U. 2011 An all-photonic molecule-based D flip-flop. *J. Am. Chem. Soc.* **133**, 20742–20745.

89. Liu, Y., Jiang, W., Zhang, H. Y. & Li, C. J. 2006 A multifunctional arithmetical processor model integrated inside a single molecule. *J. Phys. Chem. B* **110**, 14231–14235.

90. Gotor, R., Costero, A. M., Gil, S., Parra, M., Gaviña, P. & Rurack, K. 2013 Boolean operations mediated by an ion-pair receptor of a multi-readout molecular logic gate. *Chem. Commun.* **49**, 11056–11058.

91. Vester, M., Staut, T., Enderlein, J. & Jung, G. 2015 Photon antibunching in a cyclic chemical reaction scheme. *J. Phys. Chem. Lett.* **6**, 1149–1154.

92. Vester, M., Grueter, A., Finkler, B., Becker, R. & Jung, G. 2016 Biexponential photon antibunching: Recombination kinetics within the Forster-cycle in DMSO. *Phys. Chem. Chem. Phys.* **18**, 10281–10288.

93. Sehgal, R. K. & Kumar, S. 1989 A simple preparation of 1-hydroxypyrene. *Org. Prep. Proced. Int. New J. Org. Synth.* **21**, 223–225.

View Article Online
DOI: 10.1039/C6PP00290K

Tables

Table 1: Spectroscopic properties of **1**-**3** at physiological pH (pH = 8), for spectroscopy of **4** see Table 3, for other forms of **2**, see ESI S35.

	1	**2**[a]	**3**
$\lambda_{max,abs}$ [nm]	410	484	407
$\lambda_{max,em}$ [nm]	472	558	448
Φ	0.98	0.86	1.00
$\tau_{fl,\ RO^-}$ [ns]	3.89	5.81	3.73

[a] RO^--form

Table 2: Kinetic parameters for reactions of the dye system with different enzymes.

Compound	**1**	**3**	**4-MUP**	**1**	**3**	**2**	**4-MUBu**
Enzyme	**Alkaline Phosphatase**			**Acid Phosphatase**		**Porcine Liver Esterase**	
K_m [μM]	3.0	2.9	2.2	40.8	48.6	3.7	16.9
k_{cat}/K_m [1/M/s]	6.9 x 10^8	1.1 x 10^8	1.8 x 10^7	6.0 x 10^2	3.9 x 10^4	7.1 x 10^3	5.7 x 10^3

Table 3: Spectroscopic data of compound **4**.

	4
$\lambda_{max,abs}$ [nm]	418 (**4a**); 415 (**4d**); 463 (**4c**)
$\lambda_{max,em}$ [nm]	482 (**4a**); 557 (**4b**); 536 (**4c**)
pK_a [a]	6.8 (R**OH**CO_2^-); ~ 2.0 (RO^-**CO_2H**)
pK_a*[b]	4.5 (ROH**CO_2H**); -0.9 (R**OH**CO_2H)
Φ	0.85 (**4c**)
$\tau_{fl,\ RO^-}$ [ns]	5.58

View Article Online
DOI: 10.1039/C6PP00290K

[a] determined via absorption titration (for details, see ESI S32-S35), [b] determined by fluorescence titration (for details, see ESI S32-S35).

Table 4: Truth table for simple logic operations, 2:4 decoder (**O1**-**O4**) and Feynman gate (**O5**, **O6**) (λ_{ex} = 395 + 460 nm).

In1 (AlP)	In2 (PLE)	O1 (λ = 498 nm)	O3 (λ = 436 nm)	O2 (λ = 576 nm)	O4 (λ = 528 nm)	O5 (λ = 553 nm)	O6 (λ = 509 nm, negative logic)
0	0	1	0	0	0	0	0
1	0	0	0	1	0	1	1
0	1	0	1	0	0	0	1
1	1	0	0	0	1	1	0
gate (isolated)		**NOR**	**INHIB2**	**INHIB2**	**AND**	**YES**	**XOR**

Table-5: Truth table for operation of **4** as Feynman gate (λ_{ex} = 395 nm).

In I (low amount OH^-)	In II (high amount OH^-)	O I (λ = 514 nm, neg. logic)	O II (λ = 548 nm)
0	0	0	0
1	0	1	1
0	1	0	1
1	1	1	0
gate (isolated)		**YES**	**XOR**

View Article Online
DOI: 10.1039/C6PP00290K

Figure and scheme captions

Scheme 1: Synthesis of **1**-**4**.

Figure 1: (a) Normalized fluorescence emission of **1** (10^{-5} M, pH = 8) recorded 3 hours after incubation (enzymes in nanomolar concentration); (b) Schematic overview of spectral and molecular changes upon enzymatic conversion and corresponding K_m and k_{cat}/K_m values; (c) Different metabolic states of **1,** visualized by blacklight fluorescence excitation (λ_{ex} = 365 nm).

Figure 2: Pseudo colored fluorescence microscopic images of several cell clusters incubated with **1** and excited at λ_{ex} = 800 nm: (a-d) L929 cells, 1 h (a, c) and 3 h (b, d) after incubation, blue channel (a, b): λ_{det} = 435-485 nm (detection of compound **1**), yellow channel (c, d): λ_{det} = 535-612 nm (detection of compound **2**); (e-h) L929 cells, 1 h (e, g) and 3 h (f, h) after incubation, green channel (e, f): λ_{det} = 500-530 nm (detection of compound **4**), yellow channel (g, h): λ_{det} = 565-615 nm (detection of compound **2**).

Figure 3: (a) pH-titration of compound **4** (λ_{ex} = 395 nm); (b) Different protonation states of **4** in the ground and excited state. The color refers to the spectra in (a).

Figure 4: (a) Fluorescence spectra (normalized to substrate fluorescence, λ_{ex} = 395 + 460 nm (see ESI S48), substrate concentration: 10^{-5} M, tris-HCl buffer solution at pH = 8) with corresponding output channels and threshold levels for (a) several logic operations (O1-O4) and (b) Feynman gate (O5, O6); (c) Logic circuit for the Feynman gate.

Figure 5: Fluorescence emission of **4** at different pH values (λ_{ex} = 395 nm), output channels and corresponding threshold values for molecular logic.

View Article Online
DOI: 10.1039/C6PP00290K

Scheme 1

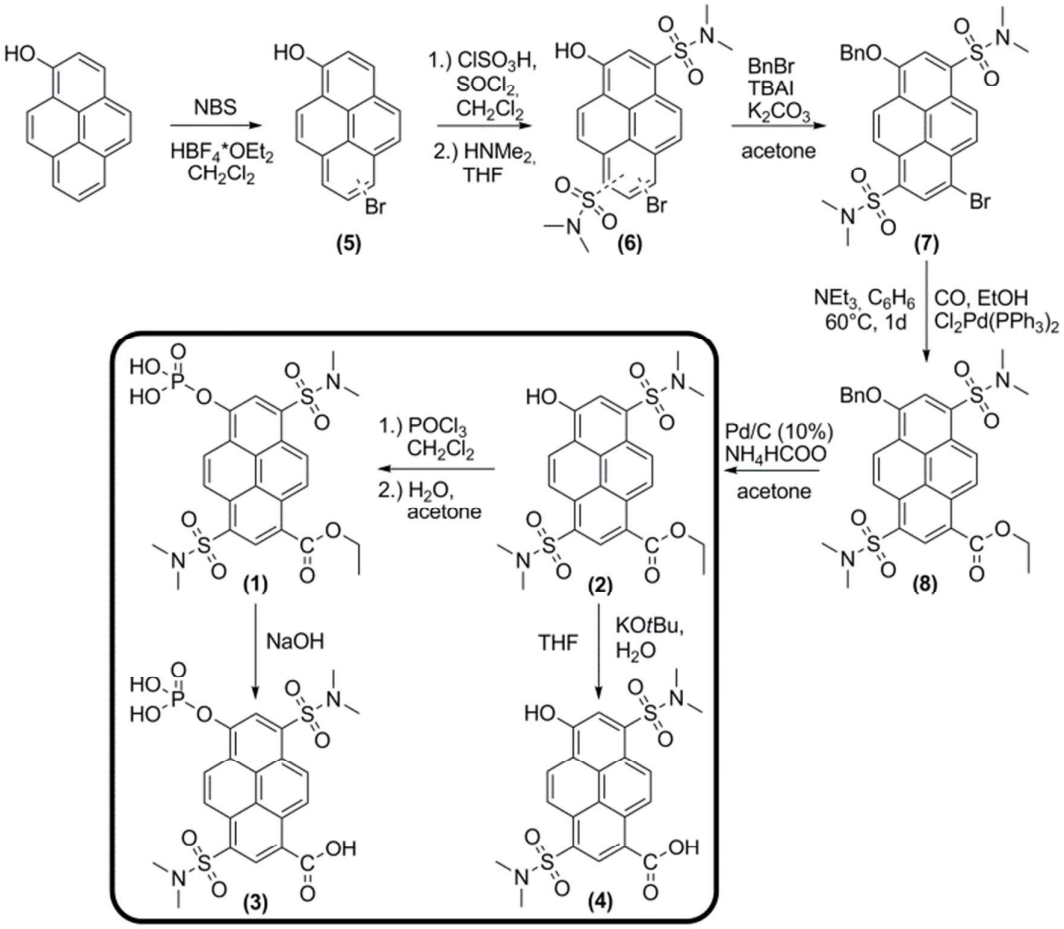

View Article Online
DOI: 10.1039/C6PP00290K

Figures

Figure 1

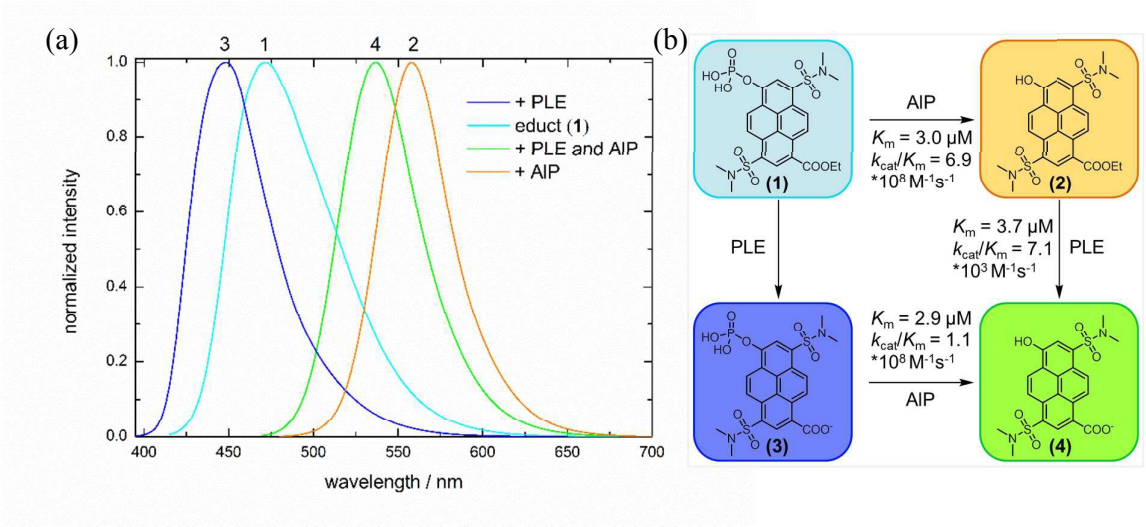

View Article Online
DOI: 10.1039/C6PP00290K

Figure 2

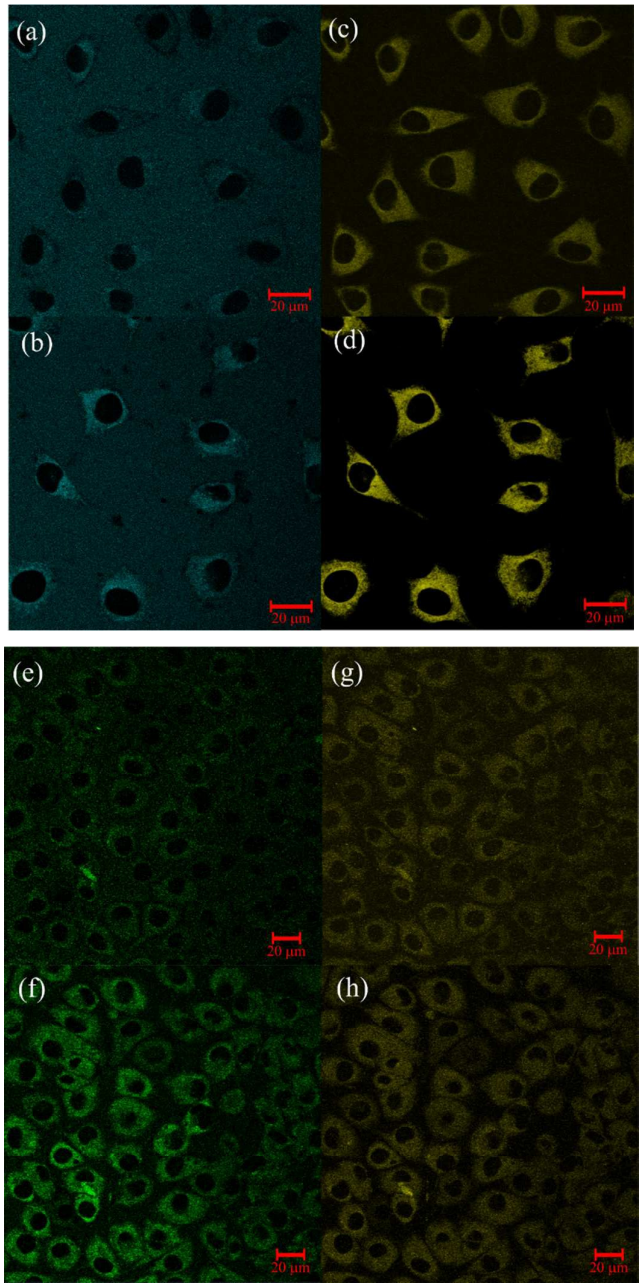

View Article Online
DOI: 10.1039/C6PP00290K

Figure 3

(a)

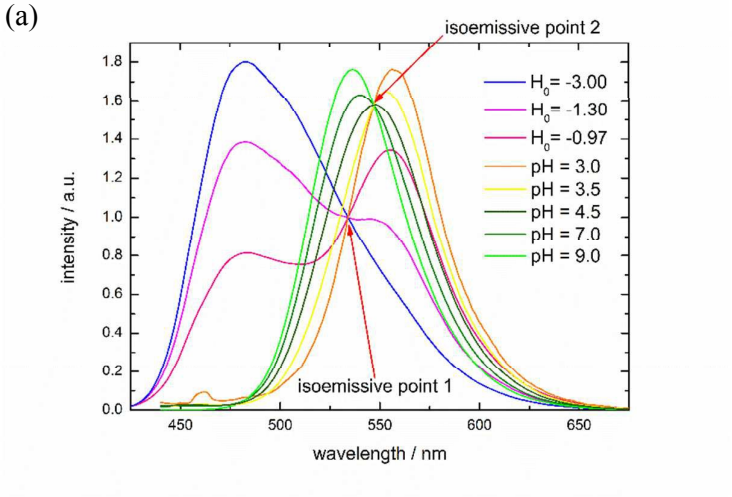

(b)

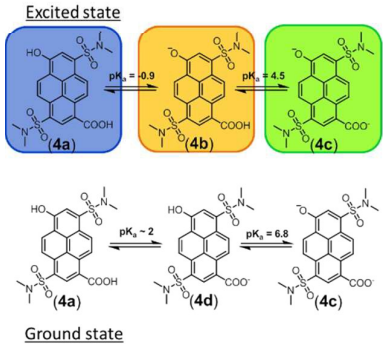

View Article Online
DOI: 10.1039/C6PP00290K

Figure 4

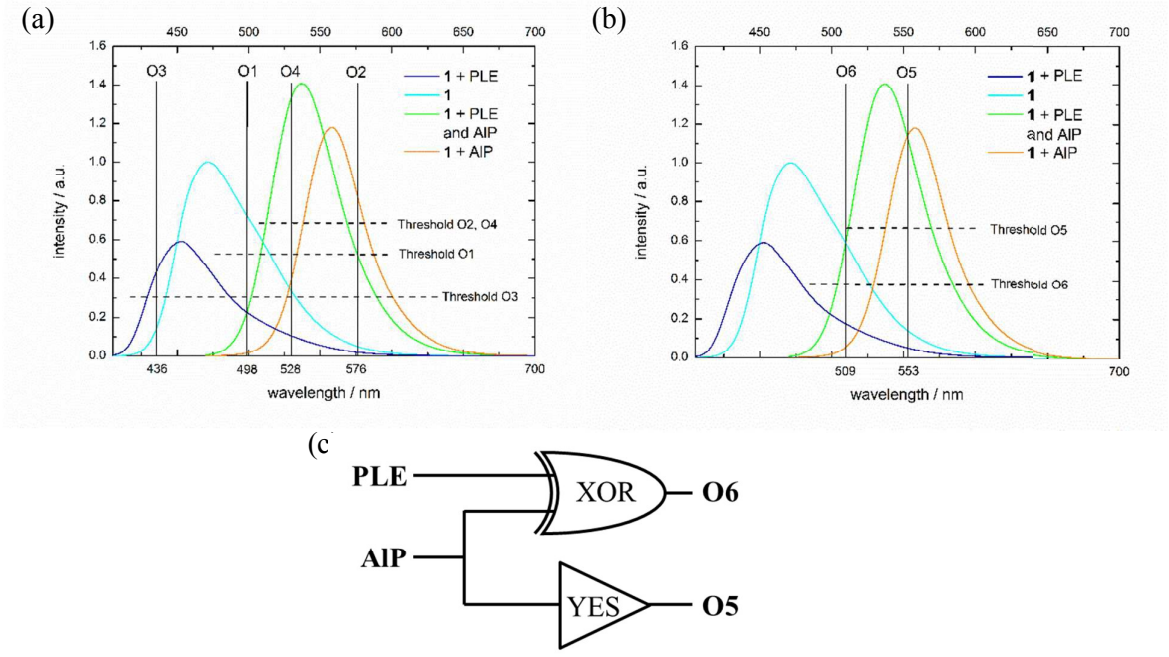

View Article Online
DOI: 10.1039/C6PP00290K

Figure 5

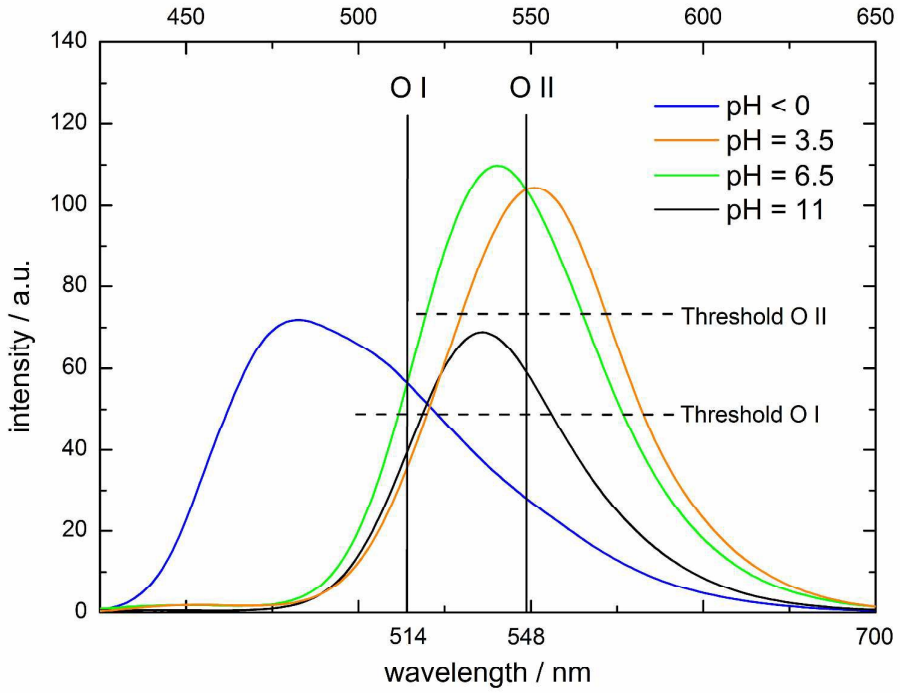

View Article Online
DOI: 10.1039/C6PP00290K

TOC

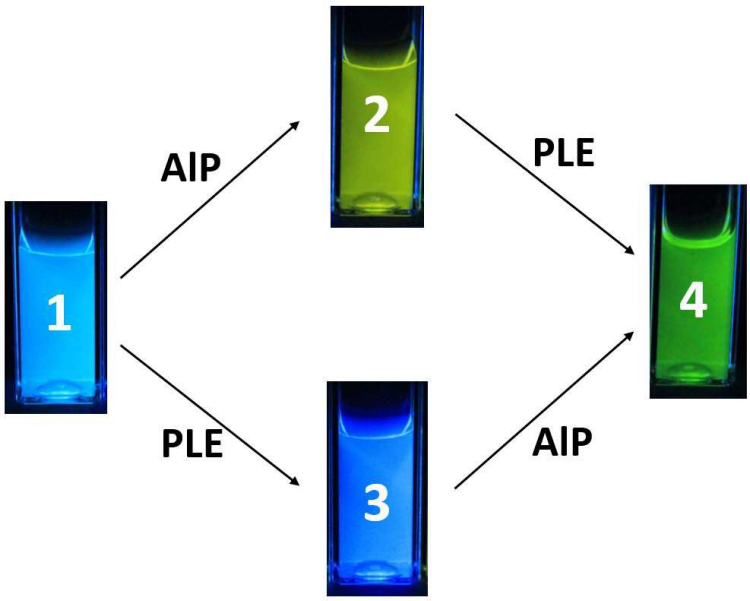

Chameleons in a test tube: Up to four easily distinguishable emission colors result from conversion by two hydrolytic enzymes at opposite reaction sites.